High-throughput superconducting T_c predictions through density of states rescaling

Kieran Bozier [1,*] Kang Wang [1] Bartomeu Monserrat [1] and Chris J. Pickard [1,2,†]
[1]*Department of Materials Science and Metallurgy, University of Cambridge, 27 Charles Babbage Road, Cambridge CB3 0FS, United Kingdom*
[2]*Advanced Institute for Materials Research, Tohoku University, Sendai 980-8577, Japan*

(Received 18 September 2025; revised 19 January 2026; accepted 26 January 2026; published 17 February 2026)

First-principles computational methods can predict the superconducting critical temperature T_c of conventional superconductors through the electron-phonon spectral function. Full convergence of this quantity requires Brillouin-zone integration on very dense grids, presenting a bottleneck to high-throughput screening for high-T_c systems. In this work, we show that an electron-phonon spectral function calculated at low cost on a coarse grid yields accurate T_c predictions, provided the function is rescaled to correct for the inaccurate value of the density of states at the Fermi energy on coarser grids. Compared to standard approaches, the method converges rapidly and improves the accuracy of predictions for systems with sharp features in the density of states. This approach can be directly integrated into existing materials screening workflows, enabling the rapid identification of promising candidates that might otherwise be overlooked.

DOI: 10.1103/82zm-by55

I. INTRODUCTION

The search for materials with higher superconducting transition temperatures (T_c) at ambient conditions is one of the great challenges in condensed matter physics. To date, despite decades of discovery, the majority of superconductors remain restricted to temperatures below liquid nitrogen (77 K) or require the high-pressure environment of diamond-anvil cells [1,2]. The complexity of this challenge has driven the development of sophisticated theoretical and computational tools to guide experimental efforts [3–7]. A particularly powerful approach in the search for new conventional superconductors is first-principles calculations based on density-functional theory (DFT) and Eliashberg theory [8]. By calculating the electronic structure of a crystalline material, it is possible to calculate the phonon spectrum and evaluate the electron-phonon matrix elements, which describe the strength of the coupling between the electron and phonon subsystems [9–11]. In conventional phonon-mediated BCS superconductors, the strength of this coupling determines the superconducting transition temperature [12]. The advances in calculating electron-phonon properties from DFT have made it possible to predict T_c for conventional superconductors entirely from first principles [13]. This has culminated in a string of successes in the field of high-pressure hydride superconductors, where in many cases the theoretical predictions have guided experimental discovery. Such systems include H_3S [14,15], CaH_6 [16,17], and LaH_{10} [18–23], all of which display excellent agreement between the experimental and calculated T_c.

These first-principles calculations are now commonly used alongside methods for crystal structure prediction [24], such as *ab initio* random structure searching [25–27], minima hopping [28,29], generative models [30], particle swarms [19,31], and genetic algorithms [32–34] to explore increasingly large regions of composition and pressure space for promising superconducting materials [27,29,35–37]. Many of these methods are now leveraging machine learning to accelerate these searches and explore more complex candidates [38–42]. However, high-throughput screening comes with some challenges. When screening through many hundreds or thousands of structures, the computational cost of finding the property of interest for each structure must be as low as possible. However, a fully converged first-principles calculation of the phonon and electron-phonon properties of a material requires very fine electronic **k**- and phonon **q** grids, which are prohibitively expensive [43]. Using coarser electron and phonon grids keeps the computational cost low, but can compromise the accuracy. Therefore, a balance must be achieved, between screening as many candidates as possible, and ensuring the predicted T_c from the coarse grids remains close to the converged value.

The reality is that many superconducting systems are poorly described by these coarse grid calculations. One of the most critical ingredients for a high T_c is a large density of states (DOS) at the Fermi energy, denoted N_F [1]. This is because the presence of more states at the Fermi energy allows more electrons to participate in the BCS pairing interaction [44,45]. Other factors are also important, such as high-frequency phonons leading to a large $\omega_{\log}$ in the McMillan and Allen-Dynes equations, but these tend to be subject to fundamental limits set by physical constants [46] and thus

*Contact author: kb697@cam.ac.uk
†Contact author: cjp20@cam.ac.uk

Published by the American Physical Society under the terms of the Creative Commons Attribution 4.0 International license. Further distribution of this work must maintain attribution to the author(s) and the published article's title, journal citation, and DOI.

the ability to optimize these is more limited. Consequently, most promising systems have a high density of states at the Fermi energy. This commonly occurs in proximity to a sharp peak in the density of states—although these systems do often host competing instabilities such as magnetic ordering and charge-density waves. Sharp peaks in the DOS are rarely well captured by coarse electronic grids, because in most superconductivity calculations the density of states is modeled by applying Gaussian smearings with a fixed width σ to the energy eigenvalues from the electronic grid. This method can produce inaccurate values of the density of states when the electronic grid is too coarse [47,48], leading to a direct under- or overestimation in T_c. Examples of high T_c systems with a sharp peak near the Fermi energy are H_3S [49] and the proposed candidate Mg_2IrH_6 [27,29], and both result in substantially underestimated critical temperatures when coarse grids are used. In the context of high-throughput screening, there is therefore a risk that an interesting candidate with an anomalously high density of states would be filtered out of the search at an early stage.

The importance of the density of states in the convergence of T_c was explored by Koretsune and Arita in Ref. [50]. They argue that many quantities important for superconductivity can be written in the form of the density of states multiplied by a weighted average. For many systems, they found that this average term shows only a weak dependence on the electronic-$\mathbf{k}$ grid and smearing σ, demonstrating that it is often the convergence of N_F that is responsible for the very fine grids required in T_c calculations. In a later work [51], they applied this method to the BiS_2 system to obtain an electron-phonon coupling strength λ and T_c that were almost independent of smearing, by multiplying the electron-phonon spectral function $\alpha^2F(\omega)$ by a correction factor. In this work, we directly build on these ideas, namely how describing the density of states correctly is transformative in accelerating convergence on coarse grids—with a particular focus on its importance in high-throughput calculations. By introducing a correction factor to rescale the relevant superconducting functions, as was done in Ref. [51], we have been able to accelerate convergence with respect to the Gaussian smearing width and grid sizes. Importantly, we have found the method is most effective for systems with sharp features in the density of states, which are among the most promising systems for high-temperature superconductivity.

II. THEORY

The central quantity in the calculation of the transition temperature is the Eliashberg electron-phonon spectral function $\alpha^2F(\mathbf{k},\mathbf{k}',\omega)$. This represents the average of the electron-phonon matrix elements over the allowed momentum transfers [4]. The function, which is proportional to the phonon density of states weighted by the electron-phonon matrix elements $g_{nm\nu}(\mathbf{k},\mathbf{k}')$, is given by [52,53]

$$\alpha^2F_{nm}(\mathbf{k},\mathbf{k}',\omega) = N_F \sum_{\nu} |g_{nm\nu}(\mathbf{k},\mathbf{k}')|^2 \delta(\omega - \omega_{\mathbf{k}-\mathbf{k}',\nu}). \quad (1)$$

It is linearly dependent on N_F, the density of electronic states at the Fermi energy. Here, $\mathbf{k}$ and $\mathbf{k}'$ are the electronic momenta, n, m are the electronic band indices, and $g_{nm\nu}(\mathbf{k},\mathbf{k}')$ are the electron-phonon matrix elements for the electronic states $|\mathbf{k},n\rangle$ and $|\mathbf{k}'m\rangle$ coupled by a phonon of mode ν, momentum $\mathbf{q} = \mathbf{k} - \mathbf{k}'$, and frequency $\omega_{\mathbf{k}-\mathbf{k}',\nu}$, respectively.

In the isotropic approximation, the average value of $\alpha^2F(\omega)$ for all $|\mathbf{k},n\rangle$ and $|\mathbf{k}'m\rangle$ on the Fermi surface is used. This can be obtained by inserting dimensionless weighting functions $W_{\mathbf{k}n} = \frac{\delta(\epsilon_{\mathbf{k}n})}{N_F}$, where $\epsilon_{\mathbf{k}n}$ is the energy with respect to the Fermi energy, and performing a summation over all momenta $\mathbf{k}$, $\mathbf{k}'$ and bands n, m. This leads to the more commonly seen expression [52]

$$\alpha^2F(\omega) = \frac{1}{N_F} \sum_{\mathbf{k},\mathbf{k}',n,m} \sum_{\nu} |g_{nm\nu}(\mathbf{k},\mathbf{k}')|^2 \times \delta(\epsilon_{\mathbf{k}n})\delta(\epsilon_{\mathbf{k}'m})\delta(\omega - \omega_{\mathbf{k}-\mathbf{k}',\nu}). \quad (2)$$

The function is still directly proportional to the density of electronic states at the Fermi level because each summation over $\mathbf{k}$, n of the delta functions $\delta(\epsilon_{\mathbf{k}n})$ yields a factor of N_F. The other quantity commonly used in calculations of T_c is the isotropic electron-phonon coupling strength λ, given by

$$\lambda = \int d\omega \frac{2\alpha^2F(\omega)}{\omega}, \quad (3)$$

where again, this quantity is linearly proportional to the density of states at the Fermi energy. Hence, in calculations of these quantities, the electronic states used in the Brillouin-zone integrals must be able to reproduce the correct density of states of the material. The T_c can then be found using the coupling strength, most commonly using one of either the McMillan equation [5], the Allen-Dynes equation [6], a machine-learned model [35,54], or by directly solving the Eliashberg equations [8].

To compute these functions on finite electronic $\mathbf{k}$ grids, each Dirac delta function is replaced with a Gaussian of finite width. The particular expression used in the QUANTUM ESPRESSO code [55] is given by

$$\delta(\epsilon_{\mathbf{k}n}) \to \frac{1}{\sigma\sqrt{\pi}} \exp\left(\frac{\epsilon_{\mathbf{k}n}^2}{\sigma^2}\right). \quad (4)$$

Selecting the smearing σ requires a convergence test. The Dirac-delta function corresponds to infinitesimal smearing, but on finite grids very small smearings lead to disconnected points. By comparison, overly broad smearings may converge faster but to an incorrect value, as points far from the Fermi energy are included in the summation [52]. Several methods are commonly used to select the smearing: (i) plotting T_c against smearing for different electronic grids, and the optimal value chosen as the smallest smearing where the curves do not diverge [36,56]; (ii) for high-throughput searching, plot just one of these curves and take the smallest smearing where T_c does not rapidly diverge from the large smearing values; (iii) choose the Gaussian smearing value that most closely reproduces the value of N_F found from a very well-converged density of states calculation [50], prioritizing the importance of an accurate density of states. All rely on T_c varying only slowly as a function of smearing σ, so methods that can reduce this dependence are advantageous.

This procedure of replacing the Dirac-delta function with a Gaussian is also commonly used in calculations of the

density of states [48]. However, it is not a particularly effective method, often requiring extremely dense electronic **k** grids to produce a converged plot [47]. Quantities that depend directly on the density of electronic states at the Fermi energy, such as $\alpha^2F(\omega)$, will thus often require very fine electronic grids if calculated with the Gaussian approach. The main drawback of the method is that all **k** points have the same smearing applied, meaning sharp features in the density of states corresponding to flat bands tend to become smeared out. Instead, more effective approaches are used such as adaptive smearing [57,58], extrapolative methods [47,59], or tetrahedron methods [60,61]. In this paper, we have chosen to use the linear tetrahedron method to accurately evaluate the density of states. This approach divides the Brillouin zone into tetrahedra whose vertices are points on the electronic **k** grid. The band energies are linearly interpolated between these points, which are used to perform an analytic calculation of the density of states [60–62], in an analogous way to the trapezoidal rule. In comparison to the standard Gaussian smearing approach, sharp features such as Van Hove singularities are reproduced at significantly lower electronic **k**-grid densities [63]. By taking advantage of these more effective ways of calculating N_F, it should be possible to more rapidly converge $\alpha^2F(\omega)$ and λ.

III. METHOD AND RESULTS

A. Calculation details

Calculations of the electron, phonon, and electron-phonon properties were performed with the QUANTUM ESPRESSO code [55] using the Pseudo-Dojo PBE ONCVPSP pseudopotentials [64,65]. The kinetic-energy cutoff was determined by converging the total energy to <1 meV per atom, requiring cutoffs of around 100 Ry. Except where otherwise specified, the phonons were calculated on a coarse grid with a **q**-point spacing of $(0.06 \times 2\pi)$ Å^{-1} and a coarse **k**-point spacing of $(0.02 \times 2\pi)$ Å^{-1}, which was then interpolated onto a fine electronic grid with spacing $(0.01 \times 2\pi)$ Å^{-1} to calculate the electron-phonon matrix elements $g_{nmv}(\mathbf{k}, \mathbf{k}')$ and coupling strength λ. The T_c was calculated by solving the isotropic Eliashberg equations in the constant-DOS approximation, with a fixed Coulomb pseudopotential $\mu^* = 0.125$. In principle, the value of μ^* should be calculated from the screened Coulomb interaction [52,66,67], but this is computationally challenging in high-throughput searches and so a fixed value tends to be used. Figure 1 demonstrates the influence of μ^* on the calculated T_c for the H_3S system (at 200 GPa). The calculated T_c is plotted as a function of Gaussian smearing width for different values of μ^*, using both the default and the rescaled methods. Increasing μ^* suppresses T_c for both approaches by shifting the convergence curves downward, but notably does not affect the shape of the curves.

B. Rescaling by the density of states

To accelerate convergence, we perform an accurate calculation of the density of states at the Fermi energy using the linear tetrahedron method, and use this to replace the value obtained by the Gaussian smearing. This can be performed as a postprocessing step [51], by multiplying $\alpha^2F(\omega)$ by a simple

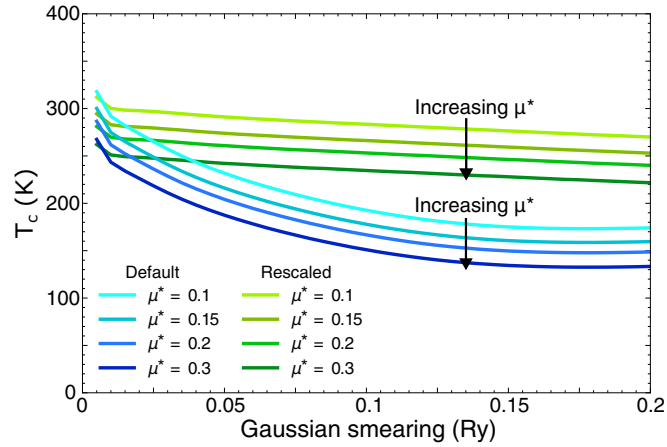


FIG. 1. The T_c of H_3S as a function of Gaussian smearing width for a range of μ^* values. The default and rescaled results are shown by the blue and green curves, respectively. Note that varying μ^* shifts the curves vertically, but preserves their convergence behavior.

prefactor:

$$\widetilde{\alpha^2F}(\omega, \sigma) = \frac{\widetilde{N_F}}{N_F(\sigma)}\, \alpha^2F(\omega, \sigma), \tag{5}$$

where $\widetilde{N_F}$ is a high-quality density of states calculated with the tetrahedron method, $N_F(\sigma)$ is the density of states calculated with the Gaussian smearing used in the T_c calculation, and $\widetilde{\alpha^2F}$ is the rescaled Eliashberg spectral function. A brief schematic of the workflow is shown in Fig. 2. In the case of a very well-converged smearing DOS, this prefactor will be unity, and this procedure has no effect. However, in high-throughput calculations the T_c and Gaussian DOS will typically not be fully converged due to the cost of using a very fine electronic grid. This prefactor therefore aims to correct the error arising from a poorly described DOS. As the cost of an accurate DOS calculation is usually very small compared to the phonon calculation, and is typically already performed as part of a high-throughput screening to remove

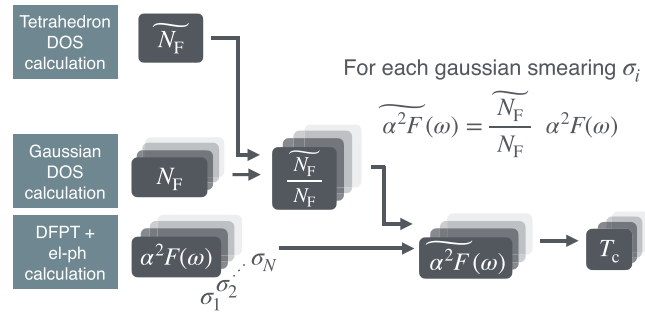


FIG. 2. Schematic of the rescaling workflow. A single high-quality linear tetrahedron calculation is performed to obtain the reference density of states at the Fermi energy, $\widetilde{N_F}$. For each Gaussian smearing width, the corresponding density of states at the Fermi energy N_F and the Eliashberg spectral function $\alpha^2F(\omega)$ are computed using the standard Gaussian smearing approach. The rescaling factor for each smearing, derived from the ratio of $\widetilde{N_F}$ to N_F, is then applied to $\alpha^2F(\omega)$ to produce the rescaled $\widetilde{\alpha^2F}(\omega)$. Finally, the transition temperature T_c is calculated from this rescaled spectral function.

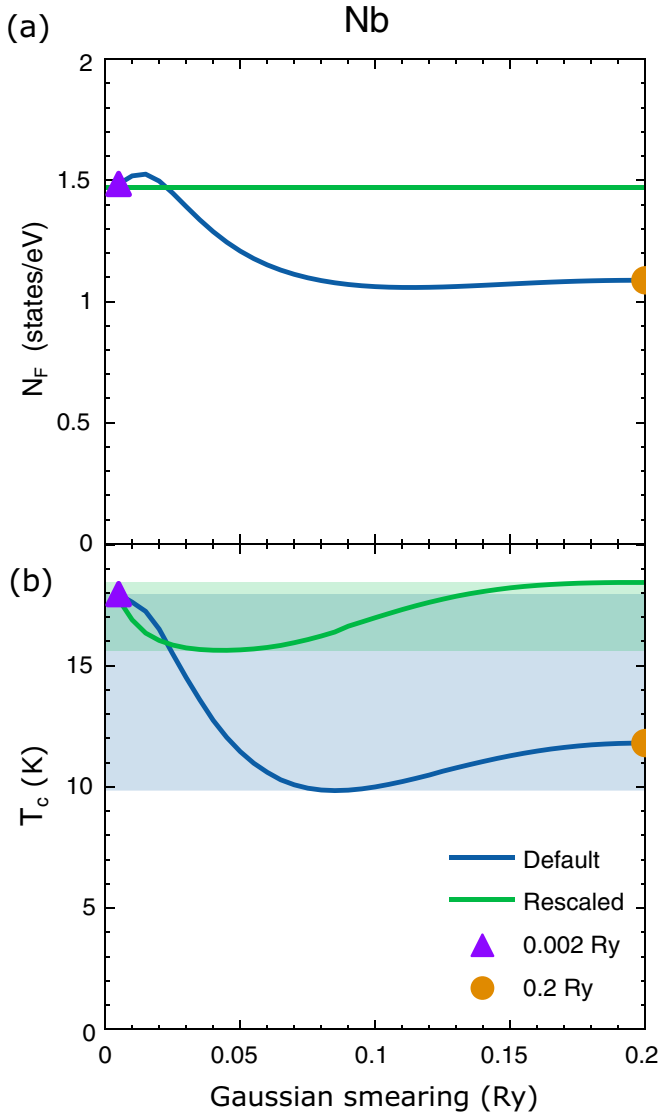


FIG. 3. The T_c is strongly dependent on the density of states at the Fermi level. In (a), the density of states at the Fermi energy N_F, and, in (b), the T_c, are plotted as a function of the smearing width of the Gaussian broadening. In (a), the blue line shows $N_F(\sigma)$ using the Gaussian smearing approach, which depends on smearing width, whereas the green line shows the value obtained with the linear tetrahedron method $\widetilde{N}_F$ (independent of smearing). In (b), the blue line represents the standard Gaussian approach, while the green line has the rescaling factor in Eq. (5) applied. The purple and orange points indicate the smearings used for the density of states in Fig. 4.

nonmetallic systems, this step can easily be incorporated into existing workflows. The rescaling method is expected to show less variation in T_c with respect to smearing σ, since the smearing dependence of N_F has been removed. Nevertheless, some variation will still remain, because smearing determines which $\mathbf{k}, \mathbf{k}'$ values in Eq. (2) are included.

C. Limitations of Gaussian smearing

Figures 3 and 4 demonstrate how an inappropriate smearing with the Gaussian approach can lead to an incorrect density of states, and consequently T_c, for niobium. In

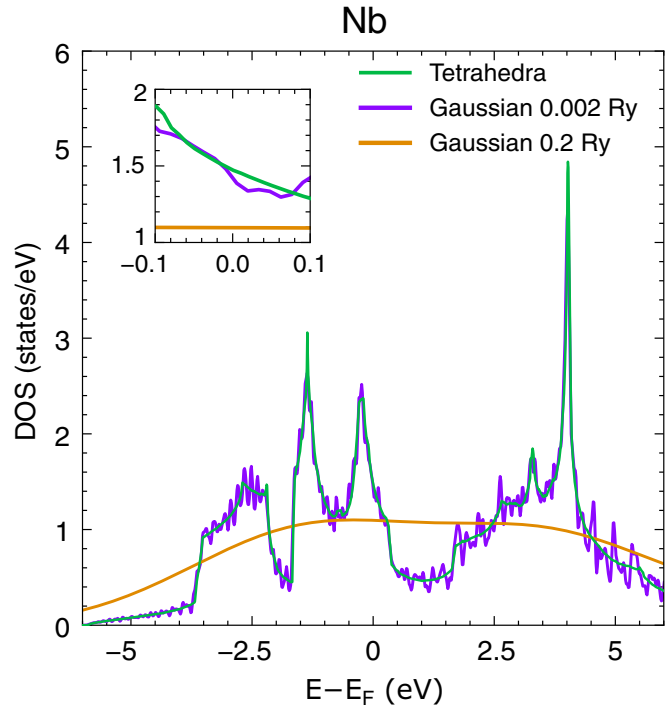


FIG. 4. The density of states of Nb is plotted for a converged tetrahedron calculation (green), and the Gaussian methods with an overly narrow (purple) and an overly broad (orange) smearing width.

subplots (a) and (b) in Fig. 3, the density of states at the Fermi level and corresponding T_c are plotted as functions of the Gaussian smearing for both the standard Gaussian method (shown in blue) and with the rescaling factor in Eq. (5) applied (shown in green). It is clear that the rescaled method displays less variation in T_c as the smearing is varied. In this example, the large smearing of 0.2 Ry leads to any sharp peaks in the DOS being smoothed out, as can be observed in the orange line in Fig. 4. As the Fermi energy in Nb lies on the downward slope of a sharp peak in the DOS, this leads to a substantial underestimation of N_F as seen in the inset, and correspondingly a lower value of T_c. If instead the Fermi energy is close to a valley, the overly smooth density of states would overestimate N_F and T_c. In comparison, if the smearing used is too small, as illustrated by the 0.002-Ry data, it can introduce spurious oscillations into smooth regions of the density of states. This is seen in the purple line of Fig. 4, particularly around 5 eV, and again can result in over- or underestimation of N_F and T_c. These oscillations arise due to insufficient sampling of the Brillouin zone, and can result in very large variations in T_c since, as the smearing is reduced, the density of states begins to resemble a set of disjointed Dirac-delta functions. For this particular system and sampling, the optimal choice of smearing parameter to reproduce the converged tetrahedron density of states is 0.025 Ry. However, it is important to note that this optimal value depends both on the sampling density, and the curvature of the DOS at the Fermi level, with denser grids and sharper features necessitating smaller smearings. In comparison to the Gaussian smearing method, where there is a trade-off between smoothness and resolution, the tetrahedron approach is able to capture both sharp and smooth features of the DOS, at comparatively coarse grid sizes.

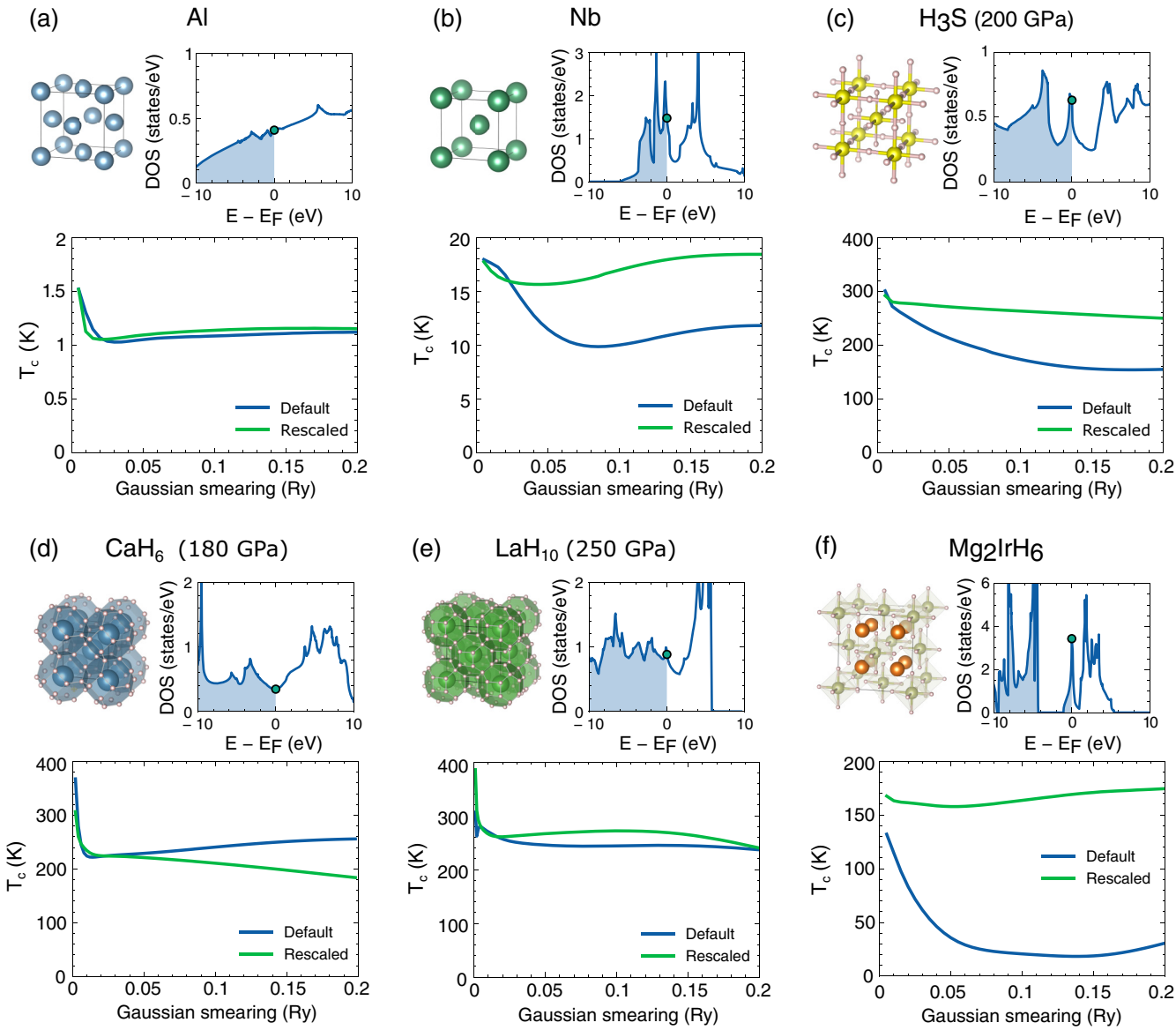


FIG. 5. The shape of the density of states at the Fermi level determines the impact of the rescaling, shown for (a) Al, (b) Nb, (c) H_3S, (d) CaH_6, (e) LaH_{10}, and (f) Mg_2IrH_6. Each panel shows the structure visualized with vesta [70], the density of states of the primitive cell calculated with the linear tetrahedron method, and the Eliashberg T_c as a function of the Gaussian smearing for the default Gaussian method and the rescaled approach. The sharper the peaks near the Fermi energy, the greater the impact of rescaling, with Mg_2IrH_6 being the system where rescaling has the largest impact.

It should be briefly noted that the obtained converged value of T_c in niobium for a $\mu^* = 0.125$ is 16 K, in agreement with other computational work [52]. However, this is notably larger than the experimental value of 9.2 K [68], which is attributed to the need for a larger μ^* value in this system [52,67]. Nonetheless, the obtained converged value of the electron-phonon coupling strength with rescaling is $\lambda = 1.4$, which is in good agreement with experimental data [69].

D. Impact of rescaling

The degree to which the rescaling impacts the T_c varies between systems, and is dependent on the shape of the density of states. Figure 5 shows a set of panels for six superconducting systems. Each panel shows the conventional cell visualized with vesta [70], a high-quality density of states calculated with the tetrahedron method on electronic grids with 60^3 points, and plots of the T_c as a function of Gaussian smearing for both the default and rescaled methods. Starting from the top left, in Fig. 5(a) we show aluminum, which is a system that is already well described by the standard Gaussian approach. The smooth density of states means that N_F is already well described even for broad smearings, resulting in a well-converged value of T_c with respect to smearing for both methods. Niobium is presented in Fig. 5(b), where the Fermi energy lies at a downward slope of a sharp peak. Consequently, the rescaling causes an increase in T_c at broad smearings, and the green rescaled curve appears to be flatter, indicating better convergence. Figure 5(c) shows H_3S, where like niobium, the Fermi energy lies near a peak and results in

an up-shift in T_c after rescaling. Additionally, the convergence plot shows the rescaled T_c is significantly less dependent on the smearing—indicating that for H_3S, the variation in the electron-phonon matrix elements is small and so convergence is dominated by how well the density of states is described. In Fig. 5(d), we see CaH_6, where the Fermi energy lies in a shallow valley of the density of states, and so a resulting minor downshift in T_c is seen at large smearings. Both methods present well converged results and are in good agreement with each other below 0.05 Ry. Figure 5(e) shows LaH_{10}, which is one of only a few systems where the rescaling arguably hinders convergence. This is discussed in Sec. IV, and is hypothesized to be due to a cancellation of errors in the default Gaussian method. Nonetheless, the high T_c for both approaches means this structure would not be missed in high-throughput searching. Last, we present Mg_2IrH_6 in Fig. 5(f), where the rescaling is at its most transformative. Here, the Fermi energy lies on a very sharp peak, which all but the smallest smearings will drastically oversmear. This results in a substantial underestimation of T_c if the standard method is used. In contrast, the rescaling easily picks out this system as having a very high T_c, with a value of about 160 K for this choice of μ^*, in very good agreement with previous studies that converged the T_c on exceptionally fine grids [27]. Importantly, in the context of structure searching and high-throughput screening, if the default methods were used with a smearing that was too broad, this structure would likely be prematurely removed from the list of promising candidates.

E. Rescaling for high throughput

There is an additional benefit to the rescaling when used for high-throughput searches: not only does it pick out systems with high values of N_F, but it often accelerates the convergence with respect to the electronic grid size. This is because in many systems, the change in N_F as the grid is varied is the dominant contribution to the convergence of T_c. As stated previously, using fine grids for calculations of λ and T_c is prohibitively expensive if applied to several hundreds or thousands of candidates. As such, a rapid convergence of T_c with respect to the phonon **q** grid and the electron **k** grid is highly desirable. To this end, we compare the T_c for different **q** (and corresponding **k** grids) for both the standard and rescaling methods. Figure 6 shows the results for H_3S. The left plot shows the T_c against smearing σ for the standard Gaussian smearing method, with a range of grid sizes ranging from a 1^3 to an 8^3 phonon grid. The coarse electronic grid used for the phonon calculation is set to twice the phonon grid density, and the fine electronic grid for the matrix element interpolation is set to 4 times the density. The right plot shows the same results, but for the rescaled method. As expected, in both methods, insufficient sampling (such as a Γ point or a 2^3 grid) leads to a wide range of values of T_c. However, for a 3^3 grid and finer, the rescaled method produces a smaller variation in T_c as a function of the smearing, and the converged value of 250 ± 10 K agrees reasonably well with other theoretical predictions in the literature [13,71]. This improvement when using the rescaling method is indicative that for the H_3S system, it is the density of states that is the limiting factor in achieving convergence. The impact is more stark for Mg_2IrH_6

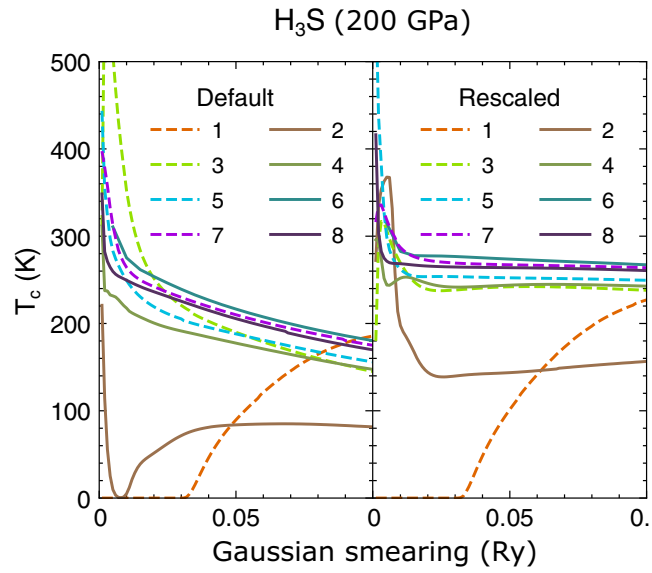


FIG. 6. Comparison between convergence of H_3S with respect to the phonon $q \times q \times q$ grid using the default method (left) and with the rescaled approach (right). The electronic grid is set to 4 times the density of the phonon grid. The rescaled method displays a noticeably faster convergence, illustrated by the flatter curves.

in Fig. 7, with even 2^3 grids reproducing the converged value of 160 K [27], and T_c is almost independent of the smearing parameter. However, an improvement is not guaranteed in all cases. In Fig. 8 we present the same convergence tests, but for the LaH_{10} system. For this system, both the standard and rescaled methods produce very similar curves, with a converged result of 250 K, in agreement with the literature [18]. This indicates that in this case the density of states is quite smooth and already well resolved even for large smearings, and so convergence is dominated instead by variations in

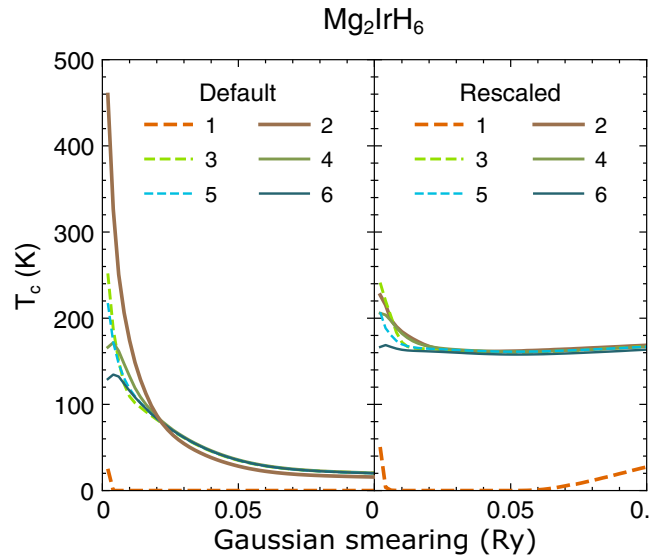


FIG. 7. Comparison between convergence of Mg_2IrH_6 with respect to the phonon $q \times q \times q$ grid using the default method (left) and with the rescaled approach (right). Here, the rescaling achieves the converged result of 160 K [27] even for a 2^3 grid.

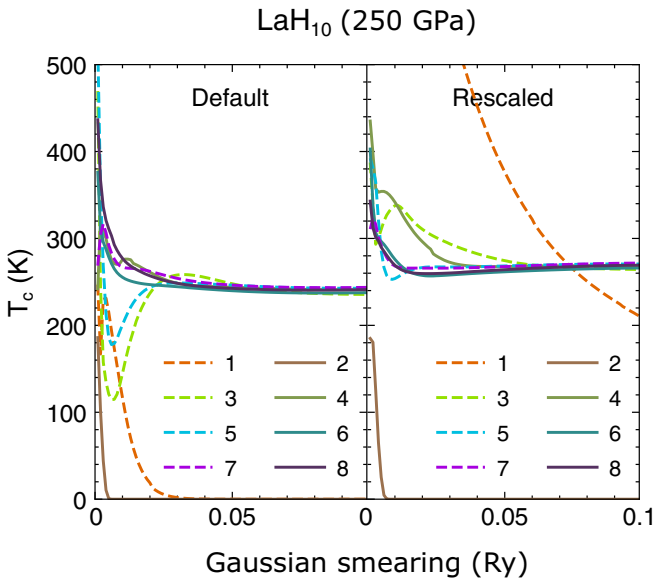


FIG. 8. Comparison between convergence of LaH_{10} with respect to the phonon $q \times q \times q$ grid using the default method (left) and with the rescaled approach (right). For this system, the rescaling does not enhance convergence.

the electron-phonon matrix elements $|g_{nm\nu}(\mathbf{k}, \mathbf{k}')|^2$, which are unaffected by the rescaling procedure.

A summary of timings and T_c estimates for the Mg_2IrH_6 system is presented in Table I. Selecting an appropriate smearing width to evaluate T_c for the default Mg_2IrH_6 curve is challenging. In comparison to the rescaled results, where T_c rapidly converges to around 160 K, the default curves lack clear plateaus or stationary points. Estimates based on the divergence of the curve yield a value of around 20 K, but this occurs at broad smearings that do not accurately reproduce the density of states. In contrast, the convergence scheme based on selecting the smearing that best reproduces the value of the density of states at the Fermi energy favors the smallest smearings, due to the sharp peak in the DOS. However, the T_c values for these smearings display significant spreads. Instead, the approach used in the table is to repeat the calculations for each phonon grid with a different electronic grid, and use the smearing where these curves diverge [36]. This tends to result in slightly more robust estimates but requires an additional Density Functional Perturbation Theory (DFPT) calculation, making it unsuitable for high-throughput approaches. In comparison to the challenge of converging with the default method, the rescaled approach rapidly reaches a value of 160 K, in agreement with previous studies for this value of μ^* [27], and displays a significantly reduced spread in T_c as the smearing is varied.

TABLE I. Table showing the wall time for the DFPT calculations for different phonon **q**-grid size for the Mg_2IrH_6 system, along with the corresponding estimates of T_c using both the default and rescaled methods. The spread is estimated by considering the range of T_c for smearings between 0.005 and 0.1 Ry. Calculations were performed on an Intel(R) Xeon(R) Gold 6142 CPU @ 2.60 GHz with 32 CPUs.

DFPT	Wall time	Default		Rescaled	
q grid	(h)	T_c (K)	Spread (K)	T_c (K)	Spread (K)
2	0.3	65	235	165.3	37
3	1.7	87	130	165.3	41
4	8.7	100	141	168.8	36
5	32.1	118	127	167.5	19
Tetra DOS	1.3				

Due to the rapid convergence of the rescaled approach, these calculations can use the 2^3-phonon **q** grid, in comparison to the 5^3 for the default method. For the DFPT calculation alone, a speedup of around 120 is achieved between the 2^3 and 5^3 grids. However, while the Gaussian DOS is already calculated in the default evaluation of λ, the rescaled method incurs an additional cost from the high-quality tetrahedron DOS calculation. This means speedups will be much more modest for systems with smooth densities of states. Nonetheless, strong accelerations are achieved in systems with sharp spectral features, such as Mg_2IrH_6, where the overall speedup remains a factor of 20 even with the additional DOS calculation.

IV. DISCUSSION

As shown earlier, the success and impact of the rescaled DOS method vary depending on the system. The method is most accurate in systems where the convergence of λ, and correspondingly T_c, is dominated by the calculated value of N_F. This corresponds to systems where the electron-phonon matrix elements $g_{nm\nu}(\mathbf{k}, \mathbf{k}')$ exhibit only weak momentum and energy dependence near the Fermi surface. In the idealized limit of constant matrix elements $g_{nm\nu}(\mathbf{k}, \mathbf{k}') = g$ and neglecting the momentum and band dependence of the phonon frequencies $\omega_{\mathbf{q},\nu} = \omega$, the expression in Eq. (3) simplifies to

$$\lambda(\sigma) = \frac{2|g|^2}{\omega} N_F(\sigma). \tag{6}$$

The only parameter dependent on smearing is N_F, so the rescaled DOS method achieves its highest accuracy, since it eliminates the error introduced by a poorly described density of states. Importantly, as discussed previously, many high-throughput workflows will calculate an accurate DOS to screen out nonmetallic systems, so this more accurate value of N_F can be used for rescaling at no additional cost.

The impact of the rescaling is determined by the shape of the density of states near the Fermi energy, and by how well this region is described by Gaussian smearing. In principle, any density of states can be replicated with sufficiently fine electronic sampling using the standard Gaussian smearing approach [57]. However, in practice, the computational constraints of high-throughput searching mean that the grid used is almost always too coarse. This causes inaccuracies in the value of N_F. Systems with smooth, broad features in their density of states, such as aluminum in Fig. 5(a), will not benefit from the rescaling, as these are already well described by broad Gaussian smearings. However, if there are sharp features, such as narrow peaks in the vicinity of the Fermi energy, then rescaling can be transformative. In the special case of Mg_2IrH_6, where the Fermi energy lies on a peak, the rescaling allows us to reproduce the converged result for this level of theory of 160 K [27] at a fraction of the cost (a speedup factor of 20 between the 2^3 and 5^3 grids when the cost of the

additional DOS calculation is included). More importantly, as seen in Fig. 5(f) and Fig. 7, without the rescaling factor the obtained T_c is far below the converged value—even for a reasonably dense grid. It is only with extremely dense grids and narrow smearings, such as those obtained with the electron-phonon Wannier code EPW [72], that the high T_c emerges when the standard method is used. Such systems with very sharp peaks at the Fermi energy are of particular importance in searches for high-T_c superconductors, as the high density of states leads to large electron-phonon coupling strengths [1]. However, the standard Gaussian smearing approach used in current workflows can significantly underestimate N_F and consequently T_c, particularly on coarse grids, meaning these promising candidates may be overlooked in the search.

Rescaling can also be beneficial for accelerating convergence with respect to grid sizes. Although the coupling strength λ on a coarse grid will generally deviate from the fine grid value—due to some $\mathbf{q}$ points being omitted from the weighted sum—in the test cases investigated the difference was within 20%. This led to estimates of T_c in Figs. 6, 7, and 8 that were largely in agreement with converged calculations in the literature, even on coarse grids. The value of rescaling here is twofold. First, the removal of the smearing dependency of the density of states typically leads to a better convergence of λ with respect to smearing, making it possible to obtain a consistent $\lambda(\sigma)$ even on coarse grids. Second, the rescaling removes the need to use very fine electronic grids to properly converge the N_F value, allowing the use of coarser $\mathbf{k}$ grids. Often a fixed ratio is used between the $\mathbf{k}$ and $\mathbf{q}$ grids, so this also means that coarser $\mathbf{q}$ grids can be used, provided the phonon properties converge relatively quickly.

It is important to note some of the limitations of the method. In certain cases, such as LaH_{10} in Fig. 5(e), the standard Gaussian method already produces convergence in T_c with respect to smearing width for relatively large (greater than 0.05 Ry) broadening. The inclusion of the rescaling factor slightly worsens the result, although the T_c is still well converged. We suggest a partial cancellation of errors may be responsible. The two sources of error are the value of the matrix elements, and their weighting given by the smeared delta functions. For the former, the finite $\mathbf{k}$-point grid means values of the matrix elements $|g_{nm\nu}(\mathbf{k}, \mathbf{k}')|$ are not directly sampled on the Fermi surface, but at points some distance away. If the value of $|g_{nm\nu}(\mathbf{k}, \mathbf{k}')|$ on the sampled points does not reflect the true value on the Fermi surface then a systematic error is introduced. In particular, at larger broadening, points increasingly far from the Fermi energy with potentially less representative values of $|g_{nm\nu}(\mathbf{k}, \mathbf{k}')|$ are included [52]. Concurrently, the actual sampling and smearing of the electronic points introduces its own error, namely, that it may not accurately reflect the true density of states at the Fermi energy. This manifests as an incorrect weighting. When the rescaling factor is applied, it will correct for the second error, but not for the first. As such, in some cases it is possible that there may be a degree of error cancellation in the standard Gaussian method, which is then not present in the rescaled method. For this reason, we recommend plotting both the standard Gaussian and rescaled methods when investigating convergence, as comparing the two gives useful insight into which factor dominates convergence. Despite this caveat, the rescaling approach has proven robust across a broad range of test systems, including simple metals, semimetals, and heavy-element systems with spin-orbit coupling.

It should also be emphasized that rescaling will not always lead to a better agreement with the experimental T_c. Sharp peaks in the density of states at the Fermi energy can cause an overestimation in T_c compared to the experimental value if rescaling is used. This is not as much a flaw with the rescaling as with the constant-DOS Eliashberg equations. These equations assume a flat DOS around the Fermi energy with a value of N_F, which the rescaling may set too high [73]. In contrast, the standard Gaussian broadened method will typically underestimate T_c in these systems as the peak in the density of states is entirely smeared out. One improvement is to use the more expensive variable-DOS Eliashberg equations [67,74], which are sensitive to the shape of the density of states around the Fermi energy. Testing with a variable-DOS method [67] tends to yield a T_c between these two extremes. As promising candidates from a high-throughput search must always be subjected to further analysis at higher levels of theory and tighter convergence before conclusions can be made, our view is it is better to overestimate these systems with pronounced peaks in the DOS at an early stage to prevent them from being prematurely screened out.

V. CONCLUSION

In summary, rescaling the Eliashberg spectral function $\alpha^2F(\omega)$ by a factor to correct the density of states is a cheap and physically motivated approach to improving the calculated value of λ and T_c. The method can enhance numerical convergence with respect to smearing parameters, and can correct for the error in T_c introduced by a poorly described density of states. The improvement is largest for systems with sharp features in the density of states at the Fermi energy, which is the case for many high-T_c systems. These improved predictions, even at coarse grid sizes, allow better estimation of the T_c and ensure promising candidates are not screened out during high-throughput searching.

ACKNOWLEDGMENTS

We thank P. I. C. Cooke and M. Caussé for many helpful discussions. K.B. gratefully acknowledges support from the Engineering and Physical Sciences Research Council [Grant No. EP/W524633/1] through an EPSRC DTP studentship in the Department of Materials Science and Metallurgy. K.W. and B.M. received support from a UKRI Future Leaders Fellowship (Grant No. MR/V023926/1). B.M. also acknowledges support from the Gianna Angelopoulos Programme for Science, Technology, and Innovation. We are grateful for computational support from the U.K. National High Performance Computing Service, ARCHER2, for which access was obtained via the UKCP Consortium and funded by EPSRC Grant No. ref EP/X035891/1.

DATA AVAILABILITY

The data that support the findings of this article are openly available [75].

[1] L. Boeri, R. Hennig, P. Hirschfeld, G. Profeta, A. Sanna, E. Zurek, W. E. Pickett, M. Amsler, R. Dias, M. I. Eremets, C. Heil, R. J. Hemley, H. Liu, Y. Ma, C. Pierleoni, A. N. Kolmogorov, N. Rybin, D. Novoselov, V. Anisimov, A. R. Oganov, *et al.*, The 2021 room-temperature superconductivity roadmap, J. Phys.: Condens. Matter **34**, 183002 (2022).

[2] C. J. Pickard, I. Errea, and M. I. Eremets, Superconducting hydrides under pressure, Annu. Rev. Condens. Matter Phys. **11**, 57 (2020).

[3] G. M. Éliashberg, Interactions between electrons and lattice vibrations in a superconductor, Sov. Phys. JETP **11**, 696 (1960).

[4] D. J. Scalapino, J. R. Schrieffer, and J. W. Wilkins, Strong-coupling superconductivity. I, Phys. Rev. **148**, 263 (1966).

[5] W. L. McMillan, Transition temperature of strong-coupled superconductors, Phys. Rev. **167**, 331 (1968).

[6] P. B. Allen and R. C. Dynes, Transition temperature of strong-coupled superconductors reanalyzed, Phys. Rev. B **12**, 905 (1975).

[7] L. N. Oliveira, E. K. U. Gross, and W. Kohn, Density-functional theory for superconductors, Phys. Rev. Lett. **60**, 2430 (1988) .

[8] E. R. Margine and F. Giustino, Anisotropic Migdal-Eliashberg theory using Wannier functions, Phys. Rev. B **87**, 024505 (2013).

[9] F. Giustino, Electron-phonon interactions from first principles, Rev. Mod. Phys. **89**, 015003 (2017).

[10] S. Baroni, S. De Gironcoli, A. Dal Corso, and P. Giannozzi, Phonons and related crystal properties from density-functional perturbation theory, Rev. Mod. Phys. **73**, 515 (2001).

[11] B. Monserrat, Electron–phonon coupling from finite differences, J. Phys.: Condens. Matter **30**, 083001 (2018).

[12] J. Bardeen, L. N. Cooper, and J. R. Schrieffer, Theory of superconductivity, Phys. Rev. **108**, 1175 (1957).

[13] D. Duan, H. Yu, H. Xie, and T. Cui, *Ab initio* approach and its impact on superconductivity, J. Supercond. Novel Magn. **32**, 53 (2019).

[14] A. P. Drozdov, M. I. Eremets, I. A. Troyan, V. Ksenofontov, and S. I. Shylin, Conventional superconductivity at 203 kelvin at high pressures in the sulfur hydride system, Nature (London) **525**, 73 (2015).

[15] D. Duan, Y. Liu, F. Tian, D. Li, X. Huang, Z. Zhao, H. Yu, B. Liu, W. Tian, and T. Cui, Pressure-induced metallization of dense $(H_2S)_2H_2$ with high-T_c superconductivity, Sci. Rep. **4**, 6968 (2014).

[16] P. Hou, Z. Huo, and D. Duan, Quantum and anharmonic effects in superconducting $Im\bar{3}m$ CaH_6 under high pressure: A first-principles study, J. Phys. Chem. C **127**, 23980 (2023).

[17] H. Wang, J. S. Tse, K. Tanaka, T. Iitaka, and Y. Ma, Superconductive sodalite-like clathrate calcium hydride at high pressures, Proc. Natl. Acad. Sci. USA **109**, 6463 (2012).

[18] F. Peng, Y. Sun, C. J. Pickard, R. J. Needs, Q. Wu, and Y. Ma, Hydrogen clathrate structures in rare earth hydrides at high pressures: Possible route to room-temperature superconductivity, Phys. Rev. Lett. **119**, 107001 (2017).

[19] H. Liu, I. I. Naumov, R. Hoffmann, N. W. Ashcroft, and R. J. Hemley, Potential high-T_c superconducting lanthanum and yttrium hydrides at high pressure, Proc. Natl. Acad. Sci. USA **114**, 6990 (2017).

[20] I. Errea, F. Belli, L. Monacelli, A. Sanna, T. Koretsune, T. Tadano, R. Bianco, M. Calandra, R. Arita, F. Mauri, and J. A. Flores-Livas, Quantum crystal structure in the 250-kelvin superconducting lanthanum hydride, Nature (London) **578**, 66 (2020).

[21] M. Somayazulu, M. Ahart, A. K. Mishra, Z. M. Geballe, M. Baldini, Y. Meng, V. V. Struzhkin, and R. J. Hemley, Evidence for superconductivity above 260 K in lanthanum superhydride at megabar pressures, Phys. Rev. Lett. **122**, 027001 (2019).

[22] I. A. Kruglov, D. V. Semenok, H. Song, R. Szczęśniak, I. A. Wrona, R. Akashi, M. M. Davari Esfahani, D. Duan, T. Cui, A. G. Kvashnin, and A. R. Oganov, Superconductivity of LaH_{10} and LaH_{16} polyhydrides, Phys. Rev. B **101**, 024508 (2020).

[23] A. P. Drozdov, P. P. Kong, V. S. Minkov, S. P. Besedin, M. A. Kuzovnikov, S. Mozaffari, L. Balicas, F. F. Balakirev, D. E. Graf, V. B. Prakapenka, E. Greenberg, D. A. Knyazev, M. Tkacz, and M. I. Eremets, Superconductivity at 250 K in lanthanum hydride under high pressures, Nature (London) **569**, 528 (2019).

[24] A. R. Oganov, C. J. Pickard, Q. Zhu, and R. J. Needs, Structure prediction drives materials discovery, Nat. Rev. Mater. **4**, 331 (2019).

[25] C. J. Pickard and R. J. Needs, Structures at high pressure from random searching, Phys. Status Solidi B **246**, 536 (2009).

[26] C. J. Pickard and R. J. Needs, *Ab initio* random structure searching, J. Phys.: Condens. Matter **23**, 053201 (2011).

[27] K. Dolui, L. J. Conway, C. Heil, T. A. Strobel, R. P. Prasankumar, and C. J. Pickard, Feasible route to high-temperature ambient-pressure hydride superconductivity, Phys. Rev. Lett. **132**, 166001 (2024).

[28] S. Goedecker, Minima hopping: An efficient search method for the global minimum of the potential energy surface of complex molecular systems, J. Chem. Phys. **120**, 9911 (2004).

[29] A. Sanna, T. F. T. Cerqueira, Y.-W. Fang, I. Errea, A. Ludwig, and M. A. L. Marques, Prediction of ambient pressure conventional superconductivity above 80 K in hydride compounds, npj Comput. Mater. **10**, 44 (2024).

[30] C. Zeni, R. Pinsler, D. Zügner, A. Fowler, M. Horton, X. Fu, Z. Wang, A. Shysheya, J. Crabbé, S. Ueda, R. Sordillo, L. Sun, J. Smith, B. Nguyen, H. Schulz, S. Lewis, C.-W. Huang, Z. Lu, Y. Zhou, H. Yang, *et al.*, A generative model for inorganic materials design, Nature (London) **639**, 624 (2025).

[31] Y. Wang, J. Lv, L. Zhu, and Y. Ma, CALYPSO: A method for crystal structure prediction, Comput. Phys. Commun. **183**, 2063 (2012).

[32] C. W. Glass, A. R. Oganov, and N. Hansen, USPEX—Evolutionary crystal structure prediction, Comput. Phys. Commun. **175**, 713 (2006).

[33] T. Ishikawa, T. Miyake, and K. Shimizu, Materials informatics based on evolutionary algorithms: Application to search for superconducting hydrogen compounds, Phys. Rev. B **100**, 174506 (2019).

[34] D. C. Lonie and E. Zurek, XtalOpt: An open-source evolutionary algorithm for crystal structure prediction, Comput. Phys. Commun. **182**, 372 (2011).

[35] M. J. Hutcheon, A. M. Shipley, and R. J. Needs, Predicting novel superconducting hydrides using machine learning approaches, Phys. Rev. B **101**, 144505 (2020).

[36] A. M. Shipley, M. J. Hutcheon, M. S. Johnson, R. J. Needs, and C. J. Pickard, Stability and superconductivity of

lanthanum and yttrium decahydrides, Phys. Rev. B **101**, 224511 (2020).
[37] E. Zurek, Hydrides of the alkali metals and alkaline earth metals under pressure, Comments Inorg. Chem. **37**, 78 (2017).
[38] C. J. Pickard, Ephemeral data derived potentials for random structure search, Phys. Rev. B **106**, 014102 (2022).
[39] P. T. Salzbrenner, S. H. Joo, L. J. Conway, P. I. C. Cooke, B. Zhu, M. P. Matraszek, W. C. Witt, and C. J. Pickard, Developments and further applications of ephemeral data derived potentials, J. Chem. Phys. **159**, 144801 (2023).
[40] A. Merchant, S. Batzner, S. S. Schoenholz, M. Aykol, G. Cheon, and E. D. Cubuk, Scaling deep learning for materials discovery, Nature (London) **624**, 80 (2023).
[41] Z. Wang, X. Wang, X. Luo, P. Gao, Y. Sun, J. Lv, H. Wang, Y. Wang, and Y. Ma, Concurrent learning scheme for crystal structure prediction, Phys. Rev. B **109**, 094117 (2024).
[42] E. V. Podryabinkin, E. V. Tikhonov, A. V. Shapeev, and A. R. Oganov, Accelerating crystal structure prediction by machine-learning interatomic potentials with active learning, Phys. Rev. B **99**, 064114 (2019).
[43] F. Giustino, M. L. Cohen, and S. G. Louie, Electron-phonon interaction using Wannier functions, Phys. Rev. B **76**, 165108 (2007).
[44] L. N. Cooper, Bound electron pairs in a degenerate Fermi gas, Phys. Rev. **104**, 1189 (1956).
[45] J. R. Schrieffer, *Theory of Superconductivity*, Advanced Book Classics (Advanced Book Program, Perseus Books, Reading, MA, 1999).
[46] K. Trachenko, B. Monserrat, M. Hutcheon, and C. J. Pickard, Upper bounds on the highest phonon frequency and superconducting temperature from fundamental physical constants, J. Phys.: Condens. Matter **37**, 165401 (2025).
[47] C. J. Pickard and M. C. Payne, Extrapolative approaches to Brillouin-zone integration, Phys. Rev. B **59**, 4685 (1999).
[48] M. Y. Toriyama, A. M. Ganose, M. Dylla, S. Anand, J. Park, M. K. Brod, J. M. Munro, K. A. Persson, A. Jain, and G. J. Snyder, How to analyze a density of states, Mater. Today Electron. **1**, 100002 (2022).
[49] Y. Quan and W. E. Pickett, Van Hove singularities and spectral smearing in high-temperature superconducting H_3S, Phys. Rev. B **93**, 104526 (2016).
[50] T. Koretsune and R. Arita, Efficient method to calculate the electron–phonon coupling constant and superconducting transition temperature, Comput. Phys. Commun. **220**, 239 (2017).
[51] C. Morice, R. Akashi, T. Koretsune, S. S. Saxena, and R. Arita, Weak phonon-mediated pairing in BiS_2 superconductor from first principles, Phys. Rev. B **95**, 180505(R) (2017).
[52] C. Pellegrini and A. Sanna, *Ab initio* methods for superconductivity, Nat. Rev. Phys. **6**, 509 (2024).
[53] P. B. Allen and B. Mitrović, Theory of superconducting *Tc*, in *Solid State Physics*, edited by H. Ehrenreich, F. Seitz, and D. Turnbull (Academic Press, New York, 1983), Vol. 37, pp. 1–92.
[54] S. R. Xie, Y. Quan, A. C. Hire, B. Deng, J. M. DeStefano, I. Salinas, U. S. Shah, L. Fanfarillo, J. Lim, J. Kim, G. R. Stewart, J. J. Hamlin, P. J. Hirschfeld, and R. G. Hennig, Machine learning of superconducting critical temperature from Eliashberg theory, npj Comput. Mater. **8**, 14 (2022).
[55] P. Giannozzi, S. Baroni, N. Bonini, M. Calandra, R. Car, C. Cavazzoni, D. Ceresoli, G. L. Chiarotti, M. Cococcioni, I. Dabo, A. Dal Corso, S. De Gironcoli, S. Fabris, G. Fratesi, R. Gebauer, U. Gerstmann, C. Gougoussis, A. Kokalj, M. Lazzeri, L. Martin-Samos, *et al.*, QUANTUM ESPRESSO: A modular and open-source software project for quantum simulations of materials, J. Phys.: Condens. Matter **21**, 395502 (2009).
[56] M. Wierzbowska, S. d. Gironcoli, and P. Giannozzi, Origins of low- and high-pressure discontinuities of T_c in niobium, arXiv:cond-mat/0504077.
[57] A. J. Morris, R. J. Nicholls, C. J. Pickard, and J. R. Yates, OptaDOS: A tool for obtaining density of states, core-level and optical spectra from electronic structure codes, Comput. Phys. Commun. **185**, 1477 (2014).
[58] R. J. Nicholls, A. J. Morris, C. J. Pickard, and J. R. Yates, OptaDOS - a new tool for EELS calculations, J. Phys.: Conf. Ser. **371**, 012062 (2012).
[59] C. J. Pickard and M. C. Payne, Second-order k · p perturbation theory with Vanderbilt pseudopotentials and plane waves, Phys. Rev. B **62**, 4383 (2000).
[60] P. E. Blöchl, O. Jepsen, and O. K. Andersen, Improved tetrahedron method for Brillouin-zone integrations, Phys. Rev. B **49**, 16223 (1994).
[61] M. Kawamura, Y. Gohda, and S. Tsuneyuki, Improved tetrahedron method for the Brillouin-zone integration applicable to response functions, Phys. Rev. B **89**, 094515 (2014).
[62] O. Jepson and O. K. Anderson, The electronic structure of h.c.p. Ytterbium, Solid State Commun. **9**, 1763 (1971).
[63] M. Y. Toriyama, A. M. Ganose, M. Dylla, S. Anand, J. Park, M. K. Brod, J. Munro, K. A. Persson, A. Jain, and G. J. Snyder, Comparison of the tetrahedron method to smearing methods for the electronic density of states, arXiv:2103.03469.
[64] D. R. Hamann, Optimized norm-conserving Vanderbilt pseudopotentials, Phys. Rev. B **88**, 085117 (2013) .
[65] M. J. van Setten, M. Giantomassi, E. Bousquet, M. J. Verstraete, D. R. Hamann, X. Gonze, and G. M. Rignanese, The PseudoDojo: Training and grading a 85 element optimized norm-conserving pseudopotential table, Comput. Phys. Commun. **226**, 39 (2018).
[66] C. Pellegrini, C. Kukkonen, and A. Sanna, *Ab initio* calculations of superconducting transition temperatures: When going beyond RPA is essential, Phys. Rev. B **108**, 064511 (2023).
[67] E. Kogler, D. Spath, R. Lucrezi, H. Mori, Z. Zhu, Z. Li, E. R. Margine, and C. Heil, IsoME: Streamlining high-precision Eliashberg calculations, Comput. Phys. Commun. **315**, 109720 (2025).
[68] D. K. Finnemore, T. F. Stromberg, and C. A. Swenson, Superconducting properties of high-purity niobium, Phys. Rev. **149**, 231 (1966).
[69] P. B. Allen, Empirical electron-phonon λ values from resistivity of cubic metallic elements, Phys. Rev. B **36**, 2920 (1987).
[70] K. Momma and F. Izumi, VESTA 3 for three-dimensional visualization of crystal, volumetric and morphology data, J. Appl. Crystallogr. **44**, 1272 (2011).
[71] I. Errea, M. Calandra, C. J. Pickard, J. Nelson, R. J. Needs, Y. Li, H. Liu, Y. Zhang, Y. Ma, and F. Mauri, High-pressure hydrogen sulfide from first principles: A strongly anharmonic phonon-mediated superconductor, Phys. Rev. Lett. **114**, 157004 (2015) .
[72] H. Lee, S. Poncé, K. Bushick, S. Hajinazar, J. Lafuente-Bartolome, J. Leveillee, C. Lian, J.-M. Lihm, F. Macheda,

H. Mori, H. Paudyal, W. H. Sio, S. Tiwari, M. Zacharias, X. Zhang, N. Bonini, E. Kioupakis, E. R. Margine, and F. Giustino, Electron–phonon physics from first principles using the EPW code, npj Comput. Mater. **9**, 156 (2023).

[73] W. Sano, T. Koretsune, T. Tadano, R. Akashi, and R. Arita, Effect of van Hove singularities on high-T_c superconductivity in H3S, Phys. Rev. B **93**, 094525 (2016).

[74] R. Lucrezi, P. P. Ferreira, S. Hajinazar, H. Mori, H. Paudyal, E. R. Margine, and C. Heil, Full-bandwidth anisotropic Migdal-Eliashberg theory and its application to superhydrides, Commun. Phys. **7**, 33 (2024).

[75] K. Bozier, K. Wang, B. Montserrat, and C. J. Pickard, High-throughput superconducting T_c through density of states rescaling [Data set], Zenodo (2025), https://doi.org/10.5281/zenodo.18519011.